Reflectionless Programmable Signal Routers

Jérôme Sol, Ali Alhulaymi, A. Douglas Stone, Philipp del Hougne

APPLIED PHYSICS

Reflectionless programmable signal routers

Jérôme Sol[1], Ali Alhulaymi[2], A. Douglas Stone[2], Philipp del Hougne[3]*

We demonstrate experimentally that reflectionless scattering modes (RSMs), a generalized version of coherent perfect absorption, can be functionalized to perform reflectionless programmable signal routing. We achieve versatile programmability both in terms of operating frequencies and routing functionality with negligible reflection upon in-coupling, which avoids unwanted signal power echoes in radio frequency or photonic networks. We report in situ observations of routing functionalities like wavelength demultiplexing, including cases where multichannel excitation requires adapted coherent input wavefronts. All experiments are performed in the microwave domain based on the same irregularly shaped cavity with strong modal overlap that is massively parametrized by a 304–element-programmable metasurface. RSMs in our highly overdamped multiresonance transport problem are fundamentally intriguing because the simple critical coupling picture for reflectionless excitation of isolated resonances fails spectacularly. We show in simulation that the distribution of damping rates of scattering singularities broadens under strong absorption so that weakly damped zeros can be tuned toward functionalized RSMs.

INTRODUCTION

Signal routers, a pivotal ingredient of modern nanophotonic and radio frequency (RF) networks aimed at distributing signals to transfer information or deliver energy, struggle to date with substantial reflections upon signal injection. Besides the obvious loss in signal power, such reflections can give rise to devastating unwanted reflected signal power echoes in the network. Here, we experimentally demonstrate that simultaneous perfectly reflectionless excitation of programmable signal routers is possible at multiple frequencies that can be injected through a single or multiple channels. Our concept leverages a complex scattering system with strong modal overlap that is massively parametrized by the hundreds of in situ tunable degrees of freedom of a programmable metasurface to generate a scattering state that combines reflectionless excitation with the desired signal routing functionality. On the basis of the simple critical coupling picture of balancing excitation and decay rates of an isolated resonance (*1*–*3*), our results are unexpected because our system is strongly overdamped. However, because resonances are strongly overlapping in our system, as we explain below, differential absorption and eigenvalue repulsion can create some scattering singularities with much lower damping rates than the mean; these can be tailored to allow reflectionless excitation in combination with a desired routing functionality.

The reflectionless excitation of scattering systems is a fundamental wave scattering problem across all areas of wave engineering that has received attention from diverse perspectives. Perfect reflection suppression has been known for decades to be possible through critical coupling. The latter, although often not clearly defined, typically refers to scenarios in which one seeks to excite a scattering system with a spectrally isolated resonance via a single channel (*1*–*3*). If the excitation and decay rate of this resonance can be exactly balanced at some frequency near the resonance frequency [assuming continuous wave (CW) excitation], then there will be zero reflection. The critical coupling concept typically does not distinguish between reversible and irreversible decay mechanisms, such as radiative "loss" versus absorptive loss, respectively. If all decay mechanisms rest upon irreversible absorption, then incident waves are perfectly absorbed (*4*, *5*). Critical coupling can also be understood in terms of the even older concept in electronics of perfectly matching an input impedance to a load (or output impedance) (*6*). However, the more general problem of reflectionless excitation of complex multiresonance and/or multichannel scattering systems received little attention until fairly recently because there was no general formalism that could precisely define the conditions for reflectionless excitation.

Coherent perfect absorption

Just over a decade ago, the concept of "coherent perfect absorption" (CPA) defined the conditions for reflectionless excitations of arbitrarily complex linear scattering systems with a finite amount of loss (*7*), for the specific case of fully absorbed signals. CPA is defined on the basis of the scattering matrix S, which is a linear operator, depending on frequency, which maps input wave amplitudes in all scattering channels to output amplitudes in all scattering channels; i.e., it encodes the results of all possible scattering processes. For a finite scattering system, S can always be truncated to a finite $N \times N$ matrix. In our experiments, the asymptotic scattering channels are defined in an obvious manner through the N antennas coupled to the scattering structure, henceforth referred to as the cavity. The CPA theory describes generalized conditions under which an adapted input wavefront (the complex-valued amplitudes radiated by each of the N antennas, assumed to be mutually coherent) could be trapped and perfectly absorbed within the cavity. The requirement to observe CPA at some frequency is that S has a zero eigenvalue at that frequency and that the corresponding eigenvector is used as input wavefront, irrespective of the complexity of the cavity (e.g., isolated versus overlapping resonances). Discrete, countably infinite solutions of this type ("zeros" of the S matrix) (*8*, *9*) exist if the frequency, ω, is defined in the complex plane, but only for a real ω solution is there a reflectionless CW input wavefront at ω. The CPA condition can only be achieved if the cavity has internal loss, describing absorption within the cavity

[1]INSA Rennes, CNRS, IETR-UMR 6164, F-35000 Rennes, France. [2]Department of Applied Physics, Yale University, New Haven, CT 06520, USA. [3]Univ Rennes, CNRS, IETR-UMR 6164, F-35000 Rennes, France.
*Corresponding author. Email: philipp.del-hougne@univ-rennes1.fr

and transduction of the energy to other degrees of freedom, e.g., heat or electricity.

To achieve CPA in a cavity with loss, one must, in general, tune a parameter so that one of the complex ω solutions ends up lying exactly on the real axis at some ω_0; then, if we input the correct wavefront at ω_0, it will be perfectly absorbed. Initially, CPA was mainly studied in relatively simple cavity geometries with two channels (*10*), and the ability to interferometrically control light with light (rather than through nonlinear effects) led to proposals of CPA-based signal modulators (*11*–*15*). In the past few years, there have been a number of theoretical (*16*–*19*) and experimental (*20*, *21*) studies of the CPA effect in complex scattering geometries, often with many scattering channels. For the current work, some studies in similar systems to the current one have gone well beyond just studying such unconstrained CPA and have optimized perfectly absorbing cavities under various constraints (*22*–*26*). To achieve certain CPA-based functionalities such as secure information transmission (*22*) and analog computation (*23*), it is important to achieve CPA at a specific rather than arbitrary real frequency. However, there is no guarantee that such constraints can be successfully imposed simply by tuning a single or few parameters of a (complex) scattering system. Heuristic insights from recent experiments show that the combination of a cavity with strong modal overlap (i.e., a high density of zeros in the complex plane) with a massive parametrization (e.g., hundreds of degrees of freedom from a programmable metasurface) makes it possible to precisely impose such constraints in an in situ reprogrammable manner (*22*, *23*). A programmable metasurface is an ultrathin array of elements termed "meta-atoms" whose scattering properties can be individually reconfigured (*27*); inside a wave-chaotic cavity, a programmable metasurface enables the tailoring of the boundary conditions (*28*). Nonetheless, while constrained CPA can be applied to achieve some functions, it is not suitable for the signal routing functions studied here, precisely because CPA is defined by perfect absorption of the signal. However, a more recent generalization of the CPA concept, termed "reflectionless scattering modes" (RSMs) (*29*), provides exactly the necessary framework for understanding reflectionless signal routing in complex, tunable cavities.

Reflectionless scattering modes

The RSM theory defines the conditions for reflectionless excitation of arbitrarily complex linear scattering systems (with or without internal loss) through $N_{in} \leq N$ of the N scattering channels (the case $N_{in} = N$ corresponds to CPA and will not be our focus below). Because our aim is to route signals "forward" into particular output ports, each functionality will define a set of N_{in} input ports, where the signals enter, and a set of $N - N_{in}$ output ports, where the signals exit, with zero reflection back into the input ports. RSM theory constructs an $N_{in} \times N_{in}$ submatrix of S, denoted as R_{in}, and searches for its eigenvectors with eigenvalue zero. Like in CPA, typically, a countably infinite set of solutions exist in the complex ω plane, constituting a different complex spectrum than the S matrix zeros (*30*); we refer to these solutions as "R zeros" (*29*, *31*). As noted, only if an R zero lies on the real axis does there exist a CW adapted wavefront for reflectionless excitation through the chosen N_{in} channels. We refer specifically to such real ω solutions as RSMs. The incident signal energy of an RSM is partially or fully scattered into the output ports, depending on whether the cavity has internal loss or not.

Precursors of the RSM concept already highlighted that special symmetries, such as parity-time (*PT*) symmetry, can drastically improve the accessibility of RSMs (*30*, *32*). For general systems without such symmetries, tuning is necessary to ensure that one of the R zeros lies somewhere on the real axis and becomes an RSM. However, zero reflection at a single arbitrary frequency alone is rarely a desired functionality if there are multiple output ports; instead, one would like to steer signals at specific frequencies in specific ways, typically simultaneously at multiple frequencies, e.g., for demultiplexing. Because this is a linear theory, one can aim to optimize the system simultaneously for different target behaviors at distinct frequencies. We show in the current work that a massively parametrized metasurface-programmable cavity with strong modal overlap allows us to build desirable routing functionalities upon RSMs, something not shown previously, either theoretically or experimentally. As noted, even finding RSMs in our highly overdamped cavity is unexpected and cannot be explained by the critical coupling concept. Hence, we have also performed substantial numerical simulations in this regime of overlapping resonances to confirm that RSMs exist in such overdamped systems.

Signal routing in nanophotonics and acoustics

Independent of this strand of research on perfectly reflectionless excitations under complex scattering, nanophotonics and acoustics research groups have set out to design signal routing devices. A prototypical example is a wavelength demultiplexer that splits an input signal composed of two superposed frequencies into two single-frequency outputs. For a fixed pair of operating frequencies, topology-optimized designs of refractive index patterns in integrated photonic devices have been proposed to achieve this signal routing functionality (*33*, *34*). However, once fabricated, the operation of these devices is fixed to a specific frequency pair and signal routing functionality, and they have the drawback of not being based on any general or intuitive understanding. A significant advance for programmable signal routing was made in (*35*), which projected a light pattern onto a multimode waveguide to locally alter the refractive index and thereby imprint a desired scattering topology. The projected patterns were massively parametrized by a digital micromirror device and could be reprogrammed to route a single-frequency input to a desired output channel. This work emphasized the advantage of the massive parametrization to provide enough tunable degrees of freedom, in contrast to tuning with a few thermal or electro-optic elements (*36*–*39*), and is similar in spirit to the massive programmable-metasurface parametrization used in the current work. The propagation loss in the massively parametrized multimode waveguide was very low. Unlike our metasurface-parametrized cavity, the parametrization of the waveguide was seemingly linear without significant multiple scattering or backreflection. However, the reported routing functionalities were limited to a single frequency. Moreover, for all of the here-discussed static and programmable nanophotonic signal routers, low reflection upon injection (low insertion loss) was, of course, a design goal, but the proposed designs did not achieve very high reflection suppression nor did they establish the conceptual link to the theory of reflectionless scattering.

Meanwhile, subwavelength resonant acoustic structures were used to perform wave routing functionalities that were controlled

by an adapted input wavefront (*40*–*42*), following the above-mentioned idea of "controlling light with light" (*11*–*15*). These works differ from ours chiefly in that the input wavefront rather than the scattering system determines the wave routing functionality, relegating the functionality control to wave sources that must offer multichannel coherent control. Moreover, these systems can only implement specific rather than arbitrary routing functionalities at a single frequency. While their operation is reflectionless in the ideal structures treated in analytical calculations, corresponding experiments struggle to achieve very high reflection suppression because these systems have only limited or zero capability of in situ corrections for fabrication inaccuracies.

RSM-based signal routing

Here, we experimentally demonstrate reflectionless programmable signal routers based on a wave-chaotic scattering system that is massively parametrized by a programmable metasurface. Our system's high modal density combined with the hundreds of tunable degrees of freedom allows us with unprecedented precision to impose simultaneously deep suppression of all reflections and of all undesired transmissions at multiple arbitrary desired frequencies while also generating maxima in the transmission into the desired ports. Moreover, our system's inherent programmability allows us to toggle in situ between configurations optimized for different pairs of operating frequencies and signal routing functionalities. We experimentally confirm the perfectly reflectionless routing with in situ observations of the power exiting our system through all connected channels upon direct simultaneous excitation at two frequencies through one or multiple channels.

The fundamental mechanism of the reflection suppression is a complicated, tunable destructive interference at the input ports arising from the multiple scattering of the input wavefront within the cavity. Before this work, there was no significant study in either theory or experiment of whether such reflectionless programmable routing was possible. There was not even a clear theoretical understanding of whether merely observing RSMs (let alone the signal routing functionality) is possible for a highly overdamped cavity, where the internal cavity damping far exceeds the total output coupling. We show below that the simple critical coupling picture fails under these conditions and our simulations of the R zero spectrum of a model for a cavity similar to ours give insight into why RSMs exist. While the mean imaginary part of the spectrum of R zeros is very large (and negative) for a highly overdamped cavity, the distribution of R zeros broadens in the overdamped regime, making it relatively easy to tune zeros very close to the real axis. The universality of the analytic properties of scattering operators implies that our approach to reflectionless programmable signal routing can be applied to other complex scattering systems (multimode waveguides, quantum graphs, etc.), other techniques for massive parametrization, and other wave phenomena (acoustics, elastics, optics, and quantum mechanics).

RESULTS

Unconstrained RSMs in strongly overdamped systems

To start, we examine the possibility of observing unconstrained RSMs in our experimental setup depicted in Fig. 1B. This is a precondition for being able to program additional output functionality into the system and is not trivial from the theoretical perspective, as discussed above. We also want to confirm that the qualitative behavior is consistent with the general RSM theory. Our scattering system consists of an irregularly shaped three-dimensional metallic enclosure that is parametrized by 304 1-bit programmable meta-atoms (see Methods and note S1 for details). Four single-mode guided channels are coupled to the scattering system via coax-to-waveguide adapters. The scattering matrix formalism is illustrated for the example of an RSM involving $N_{\text{in}} = 2$ of $N = 4$ channels (the ones indexed 1 and 2) in Fig. 1A. As illustrated there, a wavefront $[a_1\ a_2]$ is injected through the channels indexed 1 and 2, and ideally, we impose that zero energy exits the system through these two channels, implying that the submatrix R_{in} of S involving the two injection channels, highlighted in green, has a zero eigenvalue with corresponding eigenvector $[a_1\ a_2]$. In general, given the absence of any special symmetries in our system (e.g., PT symmetry), it is unlikely that there would be an R zero sufficiently close to the real-frequency axis to generate a reflection dip that is many orders of magnitude below the background for a given random configuration of the metasurface (*22*). In nonsymmetric systems, tuning is generically necessary to move a reflection zero to the real frequency axis (*29*, *31*). (Note that the condition of zero imaginary part will never be exactly satisfied because of experimental limitations, so in the experimental context, we use the term "reflectionless" to refer to a deep dip below the background reflection, as defined below.) Moreover, there is strong nonlocalized surface absorption of microwaves in our metallic system, implying that S is highly subunitary: The enclosure's composite quality factor is 369, and the average transmission magnitude between two ports is −28.4 dB, implying that the internal loss is orders of magnitude larger than the total radiative coupling in or out of the cavity. In the simplest model of the effect of absorption on the R zeros, the distribution of zeros is simply translated downward in the complex frequency plane by the internal loss rate. If this were the case, as we discuss further below, then all R zeros would have a large imaginary component with negative sign, leading to high reflection of CW input waves, due to the overdamping impedance mismatch, and tuning would be unable to bring a zero to the real axis.

However, upon scanning a large parameter space of 10^4 random metasurface configurations and 1601 frequency points between 4.9 and 5.6 GHz with the stringent criterion for an RSM of below −65 dB of reflected power, we do find a considerable number of RSMs. Recall that, because we have four ports, $2^4 - 1 = 15$ different reflectionless boundary conditions are possible, which can be grouped according to the number of input ports, N_{in}, with $N_{\text{in}} = 4$ corresponding to CPA. Varying N_{in} allows us to check a qualitative prediction of the RSM theory. On average, the larger is N_{in}, the higher in the complex plane the R zeros lie; for instance, the zeros of the full S matrix should, on average, have a larger imaginary part than other R zeros. Hence, once we include the strong absorption damping, which moves almost all zeros below the real axis, the distribution of zeros of the full S matrix should be closer to the real axis, making it easier to tune them to the real axis (CPA), than the R zeros with $N_{\text{in}} = 3$, 2, and 1. Similarly, we would expect to find more RSMs for $N_{\text{in}} = 3$, than for $N_{\text{in}} = 2$, and so on. This is precisely what we observe in Fig. 2A: The unconstrained RSMs are more likely to arise (with tuning) for larger N_{in}. This gives us confidence in interpreting our results with the RSM theory.

Our explanation for the existence of RSMs in a highly overdamped cavity and for the trend in Fig. 2A involves the distribution

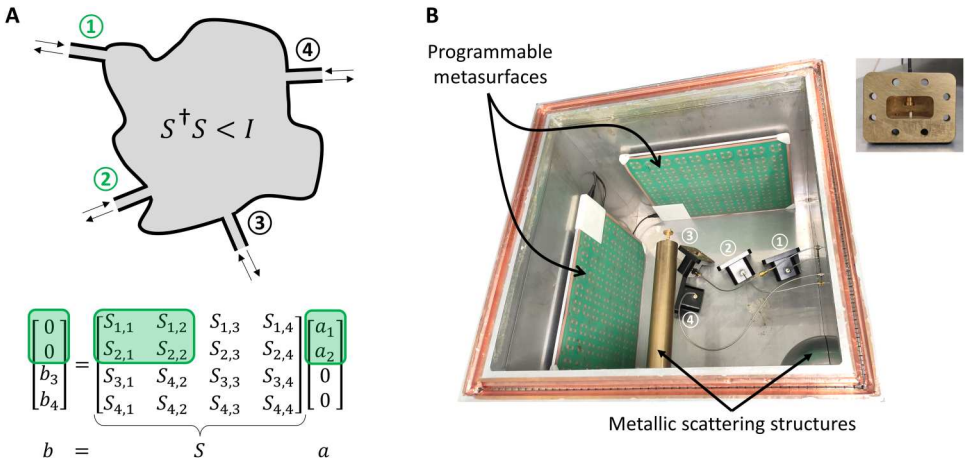

Fig. 1. RSM concept and experimental setup in a metasurface-programmable overmoded lossy scattering system. (**A**) Generic schematic of a nonunitary scattering system with four attached channels and matrix formalism corresponding to an RSM involving channels 1 and 2 (highlighted in green). (**B**) Photographic image of the corresponding experimental setup comprising a metallic electrically large scattering enclosure with irregularly shaped metallic scattering structures (top cover removed to show interior), two programmable metasurfaces composed of 152 meta-atoms each, and four waveguide-to-coax adapters to couple four monomodal channels to the system. The inset shows the front view of a waveguide-to-coax adapter.

of R zeros for different values of N_{in} and damping, which is not a quantity accessible in experiments. Hence, we study this distribution through numerical simulations of a two-dimensional chaotic cavity with three ports, as shown in the inset of Fig. 2B. Finding the complex R zero spectrum involves essentially the same techniques as finding the resonance spectrum of a complex cavity and is efficiently done in this case by a variant of the perfectly matched layer (PML) method (see Methods and note S5 for details). Using this approach, we identify all R zeros for the different possible choices of injection through $N_{in} = 3$, 2, or 1 channel(s) within a large frequency interval, as well as the poles (resonances) for which $N_{in} = 0$ and $N_{out} = 3$. We then generate statistical distributions of their imaginary parts and calculate their mean and variance. In our simulations, we can conveniently perform this analysis for different ratios of absorption rate to radiation coupling, $|\Gamma_{abs}/\Gamma_{rad}|$, by adding a finite conductivity to the walls (*28*, *43*) and varying it appropriately (see note S5).

We plot in Fig. 2B the mean and standard deviation (SD) of each of these distributions of imaginary parts for different values of N_{in} as a function of $|\Gamma_{abs}/\Gamma_{rad}|$, and we also plot the largest imaginary part observed for R zeros with $N_{in} = 3$ (zeros of the full S matrix). Our results yield three important conclusions: First, as anticipated, the mean of the distributions of imaginary components decreases monotonically as $|\Gamma_{abs}/\Gamma_{rad}|$ is increased for all considered quantities. Second, for all values of $|\Gamma_{abs}/\Gamma_{rad}|$, the means are strictly ordered and increasing for larger N_{in}, as expected from the RSM theory. Third, the SDs of the distributions of imaginary components increase monotonically as $|\Gamma_{abs}/\Gamma_{rad}|$ is increased. If this had not been the case, then one can infer from the plot that for the largest values of $|\Gamma_{abs}/\Gamma_{rad}|$ (similar to our experimental system), even the least damped CPA state would be several SDs away from the real axis, making it extremely difficult to achieve CPA (or RSM) with tuning. However, the broadening of the distributions with increasing $|\Gamma_{abs}/\Gamma_{rad}|$ implies that, despite strong overdamping, some zeros can be found in the vicinity of the real frequency axis, making tuning to find RSMs feasible. For the largest damping shown in Fig. 2B, the extremal zero for CPA is only 0.66 SDs away from the real axis. So far, we have sometimes emphasized the special case of CPA but recall that only RSMs with $N_{in} < N$ are interesting for signal routing because a CPA state with $N_{in} = N$ is defined as the irreversible perfect absorption of the signal.

One source of this broadening is due to differential absorption. Simulations detailed in note S5 show that some R zeros are more sensitive to absorption than others, leading to differential spreading of the R zero distributions along the imaginary frequency axis. The most sensitive R zeros correspond to the more localized eigenmodes, which also have higher overlap with the walls. These partially localized eigenmodes may have a semiclassical origin in terms of scars or stable periodic orbits, as discussed in note S5. Another potential source of broadening is enhanced eigenvalue repulsion as the resonances overlap more. In systems with only scattering loss, a spreading of the resonance distribution along the imaginary frequency axis has been found, as the outcoupling is increased and is associated with an effect referred to as "resonance trapping" (*44*, *45*). Similar studies of the effect of absorption loss on complex eigenvalue distributions have not been done, to our knowledge. The simulations of zero motion in the note S5 do show some apparent interactions of eigenvalues but not the marked effects found in resonance trapping models. Hence, more work is required to confirm and quantify the increase of eigenvalue repulsion for a strongly absorption-damped wave system such as ours.

Note that in our simulations, we have not performed an optimization of the cavity geometry to achieve RSMs, so the extremal values shown do not present an upper bound on the achievable imaginary component in an optimized system. Our initial studies with geometric tuning indicate that it is straightforward to generate RSMs with $N_{in} = 3$, 2, or 1 with optimization in the overdamped regime; an example with $N_{in} = 1$ is shown as inset in Fig. 2B.

So far, we have reported the first rigorous experimental observation of unconstrained RSMs in overmoded scattering systems without symmetry and provided insight into the underlying distributions that enable these observations that cannot be explained in

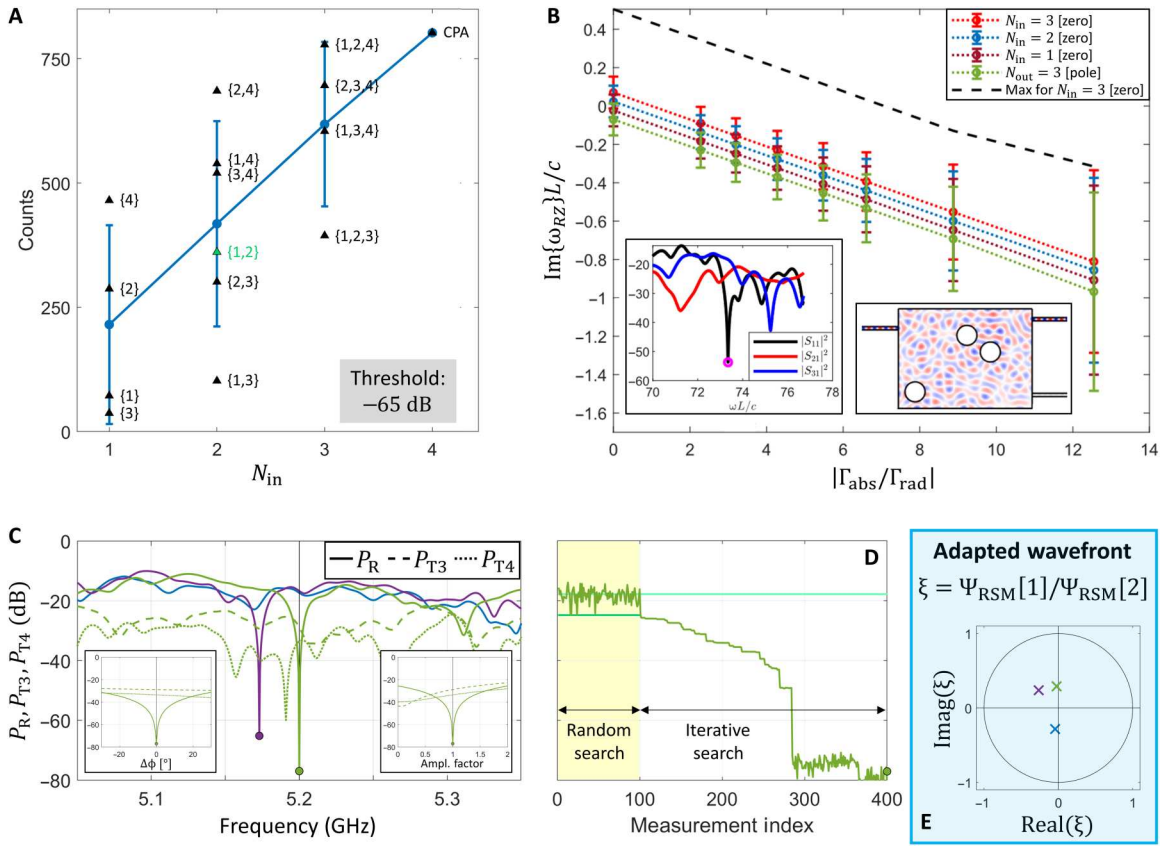

Fig. 2. Experimental observation of RSMs without and with frequency constraint. (**A**) Number of RSMs found across 10^4 random metasurface configurations and 1601 frequency points between 4.9 and 5.6 GHz. Black triangles indicate counts for specific indicated choices of N_{in} input ports; blue dots and error bars represent the average and SD across all possible choices. The labels indicate the chosen N_{in} injection channels. (**B**) Numerically determined mean and SD of the distributions of the imaginary components of zeros and poles (color coded for various choices of N_{in} and N_{out}) as a function of the ratio of absorption coupling to radiative coupling. The distributions are obtained for the cavity depicted in the inset (the color map shows the real part of an arbitrary eigenmode) within a certain frequency interval (see note S5). The black dashed line indicates the highest imaginary component for N_{in} = 3 found in the interval. (**C**) Reflected signal power P_R upon excitation through channels 1 and 2 for a random metasurface configuration (blue), for the RSM closest to 5.2 GHz out of the data from (A) (purple), and for a metasurface configuration optimized for 5.2 GHz. The dashed and dotted lines present the powers P_{T3} and P_{T4} transmitted into channels 3 and 4, respectively. The insets show the sensitivity of the RSM optimized with frequency constraint to detuning of the relative phase (left, detuned by $\Delta\phi$) or relative amplitude (right, detuned by a multiplicative scaling factor) of the two RSM wavefront Ψ_{RSM} entries. (**D**) Optimization dynamics of the frequency-constrained RSM from (C): First, 100 random metasurface configurations are tested; second, the best configuration is iteratively optimized further. (**E**) The two-channel input wavefronts corresponding to the curves in (C) are visualized in terms of the relative phase and amplitude difference using the same color codes as in (C).

terms of the simple critical coupling picture. However, as noted above, such unconstrained RSMs are not yet well aligned with practical technological needs. Thus, before closing this section, as a first step toward constrained RSMs of practical value, we consider the constraint of generating RSMs at a specific frequency and choice of input channels; we choose 5.2 GHz as the frequency and injection through the channels indexed 1 and 2 in our experimental setup. The closest RSM from our unconstrained search underlying Fig. 2A is plotted in purple in Fig. 2C and does not yield any reflection suppression at the desired frequency. However, following the approach to on-demand CPA introduced in (*22*), we can optimize the metasurface configuration to impose the desired RSM on our scattering system. To that end, we perform an iterative optimization of the metasurface configuration, as seen in Fig. 2D and detailed in the Methods and note S3. Thereby, we eventually identify a system configuration for which we have the desired {1,2}-RSM at exactly 5.2 GHz. Because we consider multichannel excitation, the reflection is only suppressed if the correct adapted wavefront (found as part of the optimization and shown in Fig. 2E) is injected. In addition to the reflected power, we also plot in Fig. 2C the power transmitted into the two remaining ports indexed 3 and 4. It is apparent that the RSM does not coincide with a zero or maximum in any of these transmissions. As stated above, frequency-constrained RSMs are hence a necessary but not sufficient condition for reflectionless signal routing.

Reflectionless wavelength demultiplexer

Our first goal is the implementation of a three-port reflectionless wavelength demultiplexer: Two frequencies f_1 and f_2 are injected without any reflection through port 1, with f_1 transmitted to port 3 but not port 2 and f_2 transmitted to port 2 but not port 3 (see Fig. 3A). This device thus involves six constraints that must be satisfied simultaneously, a major step beyond the frequency-

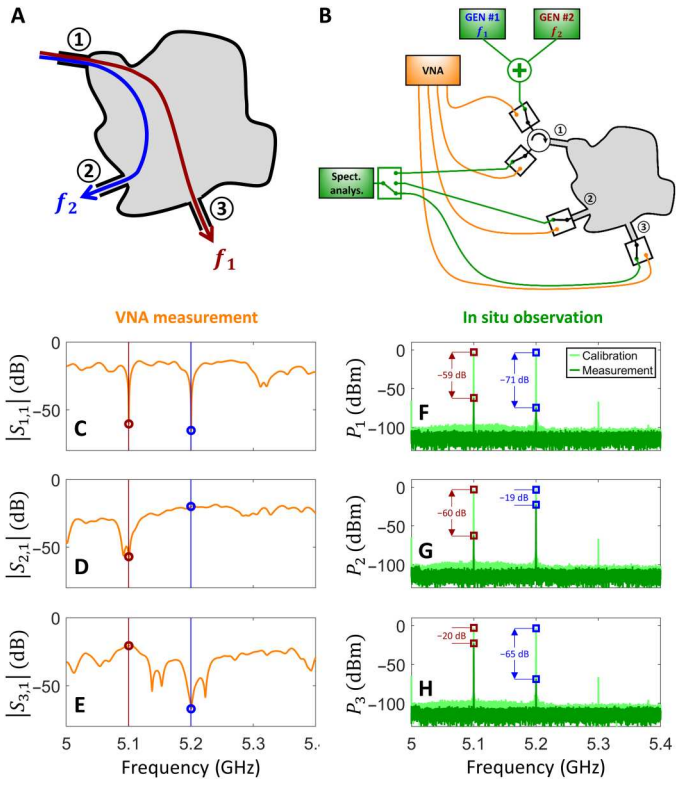

Fig. 3. Reflectionless wavelength demultiplexer. (**A**) Schematic of targeted wavelength demultiplexing functionality. (**B**) Schematic drawing of experimental setup for VNA measurements and in situ observation. (**C** to **E**) VNA measurements of the scattering parameters of the optimized system. (**F** to **H**) In situ measurements of the optimized system. CW signals at f_1 and f_2 are summed and injected through channel 1 [see (B)]. The power exiting the system through all three channels is measured and plotted in dark green. In addition, a calibration measurement to characterize losses in the cables of the measurement setup [see (B)] is shown in light green. The difference between the two curves corresponds to the in situ observed performance: reflection of at most −59 dB, undesired transmission of at most −60 dB, desired transmission of at least −20 dB, and, hence, transmission discrimination of 40 dB.

constrained RSM shown in Fig. 2C, with only a single constraint. First, two simultaneous frequency-constrained RSMs with $N_{in} = 1$ must be imposed. Here, we deliberately focus on single-channel input excitation because of its higher technological relevance (no need for very costly coherently controlled multichannel sources); however, a case of signal routing with multichannel excitation is presented in the last section of this paper. Note again that because of the strong modal overlap, these single-channel RSMs cannot be understood in terms of the simple critical coupling picture. Second, two simultaneous frequency-constrained zeros in undesired transmission must be imposed. Third, two simultaneous frequency-constrained maxima in desired transmission must be imposed. Note that constraints on transmission properties are beyond the RSM framework, which only demands zero reflection, and the general theory implying the robust existence of R zeros, as well as RSMs with tuning, does not guarantee that such solutions exist.

For this three-port experiment, we remove one waveguide-to-coax adapter from the setup seen in Fig. 1B. Because the cost function to be minimized must trade off all six constraints, we heuristically identify a suitable weighting of the six constraints as detailed in the Methods and note S3. For the experimental studies above, the functionality of interest could be extracted from measuring the S matrix on a dense grid of frequencies. Here, while we will use this approach to find optimal metasurface settings, we will demonstrate reflectionless wavelength demultiplexing in situ for our system by actually inputting the two chosen frequencies simultaneously and measuring the outputs on all channels. For this purpose, we implement a versatile measurement apparatus that can be switched between two measurement modalities (see Fig. 3B). In the first modality, we can measure our system's full scattering matrix with a vector network analyzer (VNA); in the second modality, we can inject in situ the sum of two CW signals at f_1 and f_2 and measure the spectrum of the signals exiting the scattering system through each connected channel (including the injection channel) on a spectrum analyzer. Further details about the measurement apparatus are provided in the Methods and note S1.

The frequency-dependent scattering matrix of our system, optimized to demultiplex the two frequencies 5.1 GHz and 5.2 GHz, is shown in Fig. 3 (C to E). In Fig. 3C, the sharp reflection dips characteristic of RSMs are seen exactly at the two desired frequencies. Similarly, the dips in undesired transmissions are found to be quite narrow, whereas the maxima in desired transmissions are rather broad. We conjecture that this difference in broadness originates from the fact that the transmission zeros can also be defined as spectral singularities (zeros of a scattering coefficient), although no details have been worked out for this, whereas the transmission maxima are not. The zero-scattering regime, be it for perfect suppression of reflection or undesired transmission, has intriguing effects on the delay of wave propagation through the system. Zeros of scattering coefficients that lie on the real frequency axis lead to phase singularities and anomalously long diverging delay times (*7*, *25*, *46*–*49*). The interpretation and statistical properties of complex Wigner time delays in subunitary (and possibly overmoded) scattering systems, as well as their relation to the singularities (poles and zeros) of the associated wave transport matrix, is currently an active area of research (*26*, *48*–*51*). In general, away from such singularities, it is well established that longer dwell times increase the sensitivity to minute perturbations, with important implications for precision sensing (*52*, *53*). Hence, zero scattering with diverging dwell times may imply an extreme sensitivity (*22*, *25*, *47*), provided that the waves are infinitely trapped and bouncing around without being absorbed or radiated away. We certainly observe an extreme sensitivity to frequency detuning both for zeros in reflection (guaranteed to exist by analytic properties of the S matrix) and undesired transmission.

On the basis of the corresponding in situ observations, we determine the performance metrics of our reflectionless wavelength demultiplexer. To eliminate signal loss in the measurement apparatus that is not related to the scattering system, we perform a calibration measurement without the scattering system (see Methods and note S2). The difference between in situ measurements with the optimized scattering system and the calibration measurements directly yields the performance metrics. As seen in Fig. 3F, we achieve a reflection suppression of at least −59 dB for both frequencies, justifying the terminology "reflectionless" for our signal router. At the same time, Fig. 3 (G and H) reveals that undesired transmissions are suppressed by at least 60 dB, whereas desired transmissions

are attenuated by at most 20 dB, yielding a very strong discrimination between desired and undesired transmission of 40 dB in our demultiplexer.

The 20-dB attenuation of desired transmission is not an inherent limitation of our concept but specific to the structure of our proof-of-principle experiment in which we use a strongly absorbing microwave cavity, which causes an average transmission attenuation of 28.4 dB. Given this baseline transmission attenuation, it is striking that our optimized system yields more than 8 dB of improvement on desired transmission. Ideally, of course, the attenuation of desired transmission would be negligible; simulations of lossless cavities show that optimization does still yield a good demultiplexing structure (see note S5). This goal seems certainly within reach in practice if our concept is transposed to other scattering systems with much less overall attenuation, such as the nanophotonic silicon-on-insulator device from (*35*) with almost no propagation loss. Note that some desired transmission attenuation may be tolerable in exchange for perfect reflection suppression in scenarios where the signal router is part of a network that is vulnerable to reflected power echoes. For example, in modern high-frequency RF transceiver chains, especially active components such as amplifiers are at risk of becoming unstable because of reflected power echoes. These effects can result in a complete malfunction of the entire front-end chain, which is why currently reflected power echoes are avoided by inserting additional isolators, circulators, or in-line attenuators into the chain. Isolators or circulators are bulky and costly and may involve power-consuming nonreciprocal elements such as transistors. Attenuators are reciprocal and hence also attenuate the desired signal. Similar to these considerations for RF networks, reflected power echoes negatively affect the stability of laser sources and other components in integrated photonic networks (*54*). Thus, reflectionless signal routers may be technologically attractive even if they involve attenuation of the desired transmissions because they remove the need for additional components that are currently used to suppress the consequences of reflected signals.

Programmability of reflectionless signal routers

Having implemented a specific reflectionless signal router (specific choice of operating frequencies, specific choice of routing functionality) in the previous section, we now turn our attention to the in situ reprogrammability of our system that is inherently offered by our approach. Especially for today's frequency-agile RF systems (e.g., cognitive radio), the ability to reprogram a signal router in situ so that it operates with perfect reflection suppression for a different pair of frequencies is important and valuable. We demonstrate this ability in Fig. 4A where we show in situ observations of reflectionless wavelength demultiplexing for four different pairs of operating frequencies. There is, of course, no special relation between the chosen frequencies and the geometry of our scattering system, and in principle, arbitrary frequencies could be chosen as long as they are not very close and fall into the roughly 400-MHz interval around 5.15 GHz in which our programmable metasurface can efficiently manipulate the field (see note S1). If frequency agility over an even wider range is desired in the future, then alternative metasurface designs or metasurfaces composed of meta-atoms operating within multiple bands can be deployed.

The in situ measured performance metrics of the reflectionless wavelength demultiplexing results from Fig. 4A are summarized in Table 1. For all considered choices of operating frequencies, we achieve at least −50 dB of reflection suppression and at least 34 dB in transmission discrimination. These metrics can be further improved in the future by improving the parametrization of the scattering system, e.g., through even more programmable meta-atoms, through multibit programmability of the programmable meta-atoms, etc. In addition, we also display the corresponding optimized metasurface configurations in Fig. 4A. The nonintuitive nature of these configurations due to the complex nature of our scattering system is apparent. There is also no obvious relation between the optimized patterns for different choices of operating frequencies. The different programmable meta-atom states are statistically roughly equally represented.

Another important reconfigurability feature of our system concerns the signal routing functionality. So far, we focused on wavelength demultiplexing. However, by suitably redefining the constraints, our system can also be optimized for any other input-output functionality. We demonstrate this feature in Fig. 4B for an unconventional routing functionality for which f_2 is injected through the port through which f_1 exits and f_2 exits through the remaining third port. For this routing functionality, simultaneous RSMs of f_1 and f_2 must be imposed on distinct filtered scattering matrices. The modified measurement apparatus is detailed in note S1. The in situ observations displayed in Fig. 4B and the corresponding performance metrics summarized in Table 2 (at least 52 dB of reflection suppression and at least 36 dB of transmission discrimination) confirm that both operating frequencies and routing functionality can be reprogrammed in situ while guaranteeing perfect reflection suppression.

Multichannel excitation with adapted wavefront

To this point, we have considered routers in which each frequency is injected only through a single channel; in this section, we consider the case of multichannel excitation of one of the injected frequencies. Because inputs at the same frequency from different channels will interfere, only a special adapted wavefront can be injected without reflection, as discussed previously. This multichannel case further manifests the generality of our approach, especially since much of the recent academic interest in CPA and related phenomena focused on this need for a nontrivial adapted wavefront. From a technological perspective, however, the generation of an adapted wavefront is very costly and hence unattractive. Coherent multichannel wave control requires individual phase and amplitude modulation of each source, as well as synchronization of the sources. Note that the previously discussed single-channel excitation cases are already highly nontrivial and intriguing from an academic perspective because of the strong modal overlap that leads to a failure of simple critical coupling intuition.

To study a multichannel excitation scenario, we focus on yet a different routing functionality: wavelength multiplexing. Note that time reversing a reflectionless wavelength demultiplexer does not yield a wavelength multiplexer due to the presence of absorption, which breaks the time reversal symmetry of the S matrix. Specifically, we now consider the four-port setup from Fig. 1B. The targeted device is excited with f_1 through ports 1 and 2 using wavefront ψ_{in} and with f_2 through port 3, and energy at both frequencies exits the system only through port 4. The modified measurement apparatus is detailed in note S1. The reflected power at f_1 is now defined as the sum of the powers exiting the system through the

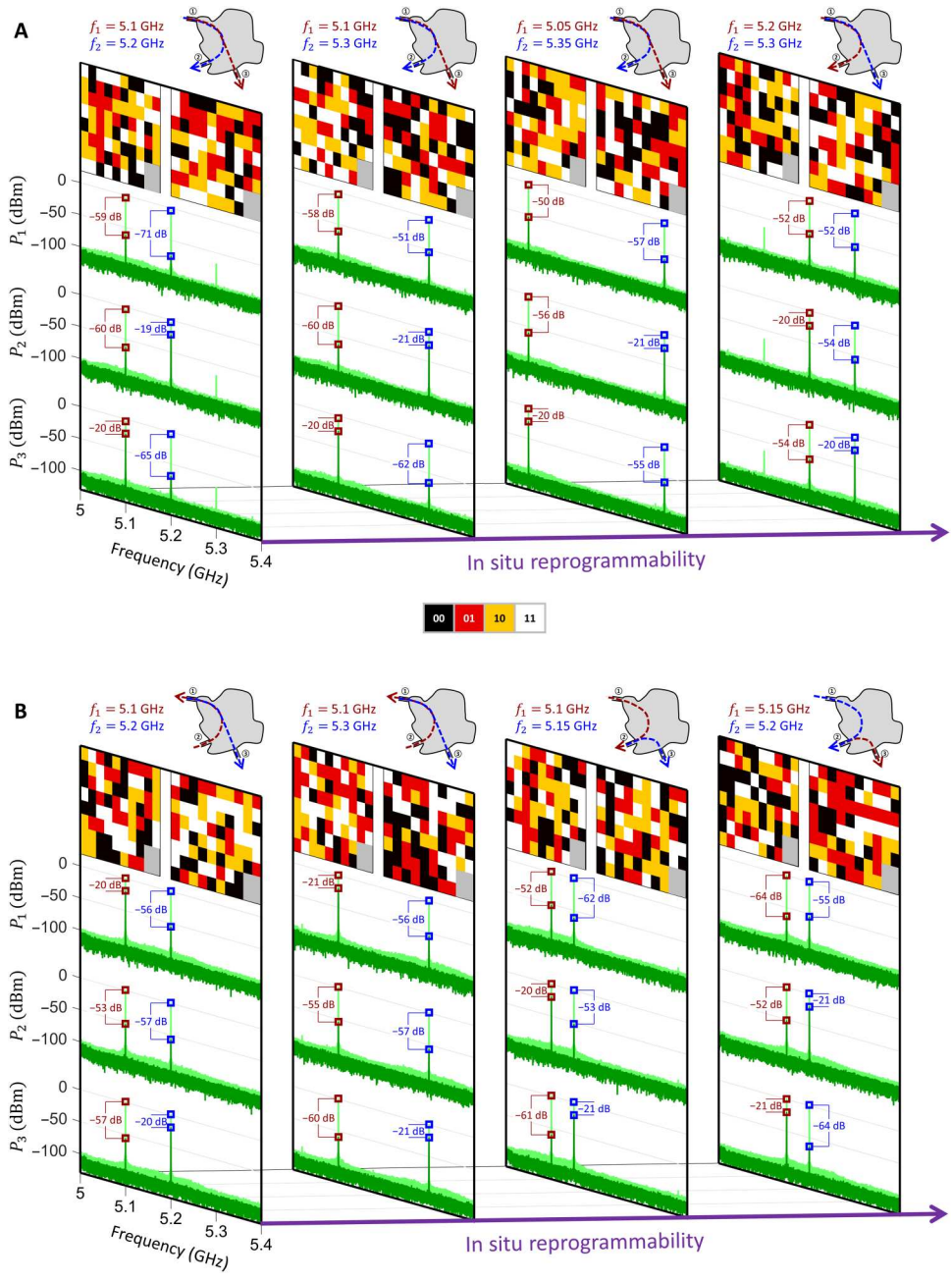

Fig. 4. Reprogrammability of reflectionless signal routing frequencies and functionality. (**A**) In situ observations of four instances of reprogramming in situ the wavelength demultiplexing frequencies by reconfiguring the programmable metasurface are shown. The first instance is that from Fig. 3. The corresponding metasurface configurations are indicated; the color code identified in the legend encodes the 1-bit programmable configuration of the meta-atom with respect to the two orthogonal field polarizations. (**B**) In situ observations of a different signal routing functionality by reprogramming the metasurface configuration. Here, f_2 is injected via the channel through which f_1 is supposed to exit, and f_2 is desired to exit through the remaining third channel. Again, four instances for different choices of f_1 and f_2 are shown.

two injection channels upon excitation with the wavefront ψ_{in} that coherently minimizes the reflection. Analogous to coherent enhanced absorption (CEA) (*55*), coherent minimized reflection (CMR) is obtained by defining ψ_{in} as the eigenvector corresponding to the smallest eigenvalue of $R^{\dagger}R$, where R now is a filtered scattering matrix involving the channels indexed 1 and 2. CMR does not distinguish between absorption and radiation loss, whereas CEA assumes that all loss is of absorptive nature. If the smallest eigenvalue of $R^{\dagger}R$ is zero, then the CMR wavefront coincides with the RSM wavefront (just as the CEA wavefront would coincide with the CPA wavefront in the case of a zero eigenvalue). Moreover, the undesirably transmitted power at f_2 is now defined as the sum of the powers at f_2 exiting the device through the channels indexed 1 and 2.

We found this optimization to be more difficult with the available tunable degrees of freedom in our experiment. On the one hand, the result from Fig. 2A suggests that a purely frequency-

Table 1. Performance metrics of the in situ-observed demultiplexer functionalities displayed in Fig. 4A. P_R, P_{Tu}, and P_{Td} denote reflected, undesirably transmitted, and desirably transmitted power.

f_1 (GHz)	f_2 (GHz)	P_R (dB)	P_{Tu} (dB)	P_{Td} (dB)	$D = P_{Td}$ (dB) − P_{Tu} (dB)
5.1	5.2	−59	−60	−20	40
5.1	5.3	−51	−60	−21	39
5.05	5.35	−50	−55	−21	34
5.2	5.3	−52	−54	−20	34

Table 2. Performance metrics of the in situ observed routing functionalities displayed in Fig. 4B.

f_1 (GHz)	f_2 (GHz)	P_R (dB)	P_{Tu} (dB)	P_{Td} (dB)	$D = P_{Td}$ (dB) − P_{Tu} (dB)
5.1	5.2	−53	−57	−20	37
5.1	5.3	−55	−57	−21	36
5.1	5.15	−52	−61	−21	40
5.15	5.2	−52	−64	−21	43

constrained RSM at f_1 may be easier to find with $N_{in} = 2$ than with $N_{in} = 1$. However, on the other hand, the simultaneous satisfaction of additional signal routing constraints may turn the multichannel advantage into a disadvantage. Moreover, undesirable transmission toward two channels rather than one channel must now be avoided at f_2. To ease the optimization burden, we allow some flexibility regarding the chosen operation frequencies in our optimization protocol. This is not a general limitation of our concept but is related to the specific constraints of our proof-of-concept experiment.

Three selected implementations of programmable reflectionless wavelength multiplexing with multichannel excitation for one of the two operating frequencies are shown in Fig. 5A. The inset illustrates the corresponding required adapted wavefronts, and Table 3 summarizes the performance metrics. We achieve good reflection suppression (at least 48 dB) and transmission discrimination (at least 30 dB). In this multichannel scenario, it is interesting to explore the sensitivity to phase or amplitude detuning of the adapted wavefront.

Table 3. Performance metrics of the in situ observed multiplexer functionalities displayed in Fig. 5.

f_1 (GHz)	f_2 (GHz)	P_R (dB)	P_{Tu} (dB)	P_{Td} (dB)	$D = P_{Td}$ (dB) − P_{Tu} (dB)
5.05*	5.245†	−52	−56	−21	35
5.245†	5.35*	−54	−51	−21	30
5.23†	5.305*	−48	−55	−21	34

*This frequency is injected through two ports (ports 1 and 2), requiring an adapted input wavefront. †This frequency is injected through a single port (port 3).

In Fig. 5B, we measure in situ how the reflected, undesirably transmitted, and desirably transmitted powers at f_1 are affected by detuning of the phase or amplitude of the adapted wavefront or detuning of the frequency. Any detuning increases the reflected power, including the (possibly at first glance unexpected) case of excitation with lower amplitude on one channel. This confirms that we have implemented a (functionalized) RSM. The undesired transmitted power can, in some cases, be slightly lower upon small detuning, implying that our optimization imposed a close-to-zero scattering condition for these undesirable transmissions, evidencing again that, in the optimizations underlying Fig. 5, it was harder to fully satisfy all six constraints simultaneously. Overall, in line with our conclusions from Fig. 3, we observe that the reflected and undesired transmitted powers are very sensitive to any type of detuning, whereas the desired transmitted power is very insensitive. This agrees with our conjecture above that a zero-scattering condition is a very narrow-band spectral singularity, while a maximum-scattering-amplitude condition can be achieved without sensitive interference and hence is less sensitive to detuning.

DISCUSSION

The need for reflectionless programmable signal routing is ubiquitous in wave engineering. Our proof-of-principle experiment is one specific implementation of our generic concept. The theory is completely general and only requires a complex cavity to serve as the routing region, massively parametrized by suitable external control knobs to explore a large ensemble of scattering matrices. Generalizations to guided or trapped waves in higher frequency regimes appear to be already within reach (*35*, *56*, *57*). Incidentally, our experimental setup maps directly into that of recently proposed metasurface-programmable wireless networks-on-chip (*43*). However, in principle, the connected channels can be guided or freely propagating in nature. For instance, one or multiple connected channels could be antennas that radiate waves to the far field. Then, on the basis of our concepts, guided waves at different frequencies can be converted to freely propagating waves radiated by specific antennas without any reflection. This use case relates to (*58*), where a variant of CMR was leveraged to feed antennas with reduced reflection; however, (*58*) did not establish the connection with well-known coherent wave control concepts, nor did they attempt to optimize or parametrize the scattering system itself to achieve reflectionless and/or programmable signal routing. It is also interesting to consider a multifunctional antenna itself as a signal router that converts incoming signals from guided monomodal waveguides [for RF antennas such as (*59*)] or from quantum emitters (for nanoantennas) to beams propagating in free space. Reflectionless conversion of signals at different frequencies into different beams, in an in situ reprogrammable manner, would be highly desirable. First attempts at improving radiation efficiency by designing the scattering environment (*60*) can be interpreted as aiming at suppressing reflections as the source couples radiation to the environment, but features such as routing and programmability are still missing. Such antenna concepts involve both guided and radiative channels, and care must be taken to ensure that the channels form an orthogonal basis. Besides the nature of the input-output channels, the scattering system itself can take diverse forms in our concept. Instead of using a chaotic cavity, our concept could, for instance, also be implemented on the basis of networks of

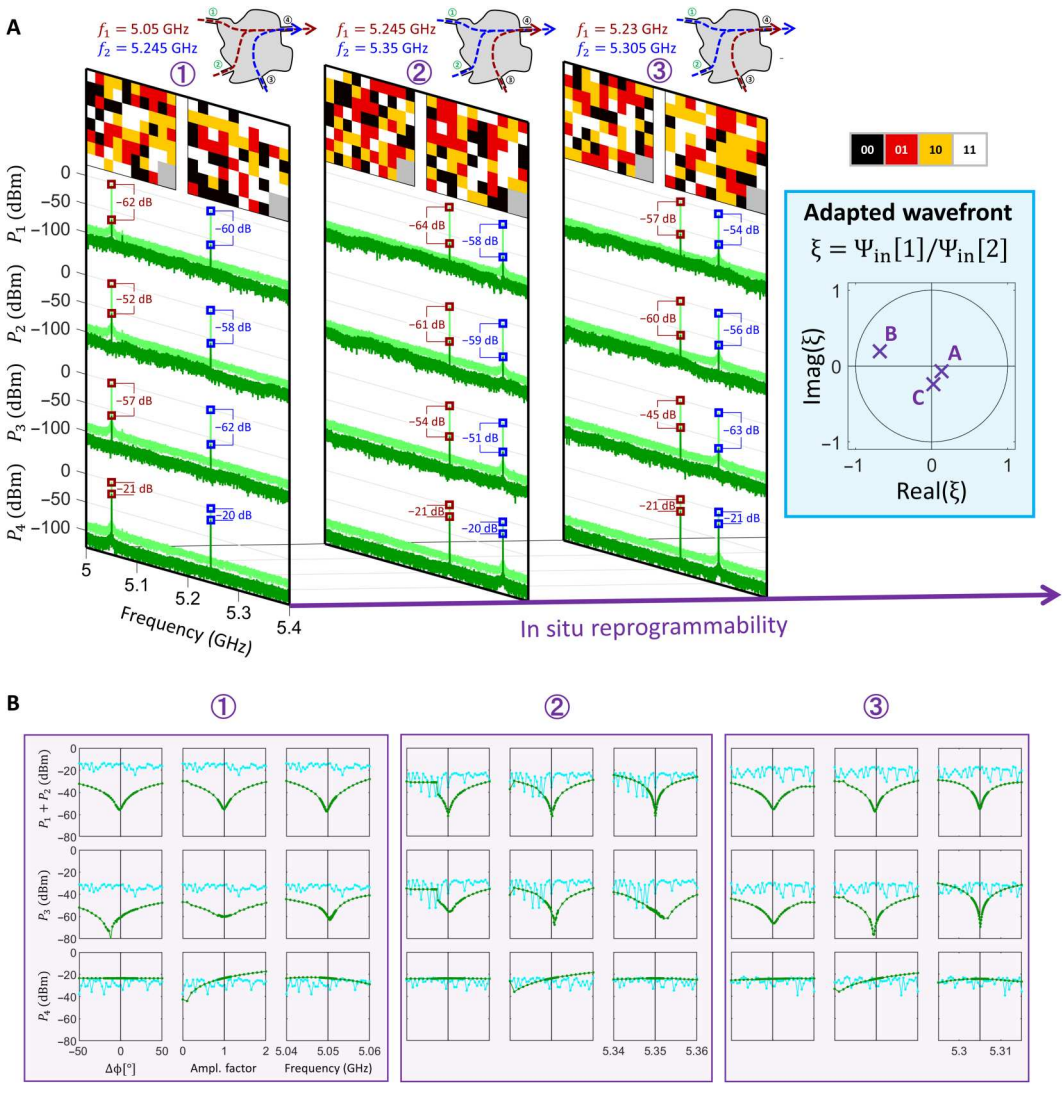

Fig. 5. Programmable reflectionless wavelength multiplexer with multichannel excitation requiring an adapted input wavefront. (**A**) Three instances of in situ observations of a reflectionless multiplexer for different pairs of f_1 and f_2, where one of the two frequencies is injected via two ports, hence requiring an adapted input wavefront. The corresponding two-channel input wavefronts are visualized in the inset in terms of the relative phase and amplitude difference. Table 3 summarizes key performance characteristics. (**B**) Analysis of sensitivity to detuning of the adapted wavefront. For each of the three instances from (A), we observe in situ how the reflected ($P_1 + P_2$), undesirably transmitted (P_3), and desirably transmitted (P_4) power varies upon detuning the relative phase (left) or amplitude (middle) of the adapted wavefront. We also check frequency detuning (right). Only results for the frequency injected through two ports are plotted (in green) in each case. The artifact upon phase detuning that is apparent in the second instance (②) originates from our coherent source's limited ability to generate arbitrary relative phase differences. We also plot (in light blue) the same three quantities as observed in situ upon injecting arbitrary random (but normalized) wavefronts; these values are for reference only, and the horizontal axes bear no relevance for them.

transmission lines such as quantum graphs (*61*) or Mach-Zehnder interferometer meshes (*62*), provided that a technique to massively parametrize them is available.

The reflectionless aspects of our signal routing concepts are based on a rigorous underlying theory, which implies that with one or a few tuning parameters, and wavefront shaping if $N_{in} > 1$, reflectionless scattering can be achieved under rather general conditions. The results in Fig. 2 confirm the expectations for RSMs within that theory. The ability to optimize RSMs for additional functionalities or with constraints does not yet have a corresponding conceptual and analytic framework, although the results shown here indicate a rather general capability to satisfy multiple additional constraints while maintaining an RSM. Specifically, it would be helpful to understand how the ability to satisfy constraints improves as a function of the number of independent tuning parameters and how this evolves as the system moves from isolated resonances to the regime of overlapping resonances studied here. These and related questions represent an important direction for future research.

Our results may appear reminiscent of open and closed channels in diffusive multiple-scattering media (*63*–*66*), but the underlying principles of our reflectionless signal routers are more general and independent of the scattering system's geometry. Open and closed

channels in diffusive media are not a resonant phenomenon: They originate from eigenvalue repulsion at each frequency, which gives rise to the bimodal distribution of eigenvalues of the system's S matrix. Therefore, in diffusive media, injection of suitable adapted wavefronts enables transmission of order unity or low transmission, respectively, at any frequency (since the frequency does not even enter the calculation to derive the bimodal eigenvalue distribution). However, such open channels do not achieve arbitrarily small reflection; the latter requires tuning of the scattering system. By tuning or optimizing the scattering system, an R zero can be placed arbitrarily close to the real frequency axis, in line with RSM theory, but this feature then only exists for a discrete frequency as opposed to at any frequency. This is because RSMs are fundamentally a resonant phenomenon and only occur at discrete frequencies, the number of which is related to the density of resonances in the system. Moreover, note that RSM theory is only based on the analytic properties of the scattering operator and makes no assumption about the system geometry being diffusive. Indeed, our experimental cavity is not a diffusive system. Hence, (functionalized) RSMs and open/closed channels are two qualitatively different phenomena, as is their underlying mathematical origin.

The perfect suppression of reflection and undesired transmission is inherently only possible at the discrete frequencies at which the zero-scattering singularities are imposed. Moreover, as seen in Figs. 3 and 5, the zero-scattering conditions are very sensitive to frequency detuning. Therefore, the bandwidth of a given signal that can be routed with perfect suppression of reflection and undesired transmission is fundamentally limited in linear passive time-invariant devices. While this is not necessarily an inconvenience for signal routers used to deliver energy with CW signals, it can be problematic for signal routers used to transfer information with modulated CW signals. Given the high density of zeros and massive parametrization of our concept, we will explore in future work the possibility of placing multiple zeros close to each other on the real frequency axis to achieve broadband near-perfect zero scattering.

Looking forward, timely research threads lay out multiple additional ideas to achieve near-reflectionless broadband programmable signal routing. First, exceptional points (EPs) of scattering zeros (as opposed to scattering poles) have a flatter frequency response than simple scattering zeros, i.e., the near-zero behavior extends over a larger band (*29*). Recent experiments (*67*, *68*) have confirmed this theoretical prediction in systems with special geometries or symmetries, but how to tune an arbitrary complex scattering system to a zero-scattering EP remains an open challenge. Second, by using nonlinear and/or active and/or time-varying systems, fundamental limitations of linear passive time-invariant systems like ours can be overcome [see (*69*) for an overview of recent work along these lines]. Third, additional opportunities may arise from modulating the input signals. For instance, zeros away from the real frequency axis can be accessed through complex-frequency excitations such that reflections are perfectly suppressed for a finite time (*70*–*72*). Carefully engineered systems may also be able to simultaneously impose zeros of different filtered scattering matrices at the same complex frequency (*73*). Fourth, there are interesting links to the recently explored use of doped epsilon-near-zero media for (not necessarily perfect) impedance matching where the dispersion of the effective permeability is tuned to tailor the bandwidth (*74*).

To summarize, we demonstrated experimentally that massively parametrized overmoded scattering systems can be tuned to functionalize RSMs such that they enable reflectionless programmable signal routing. We demonstrated with in situ observations that both operating frequencies and routing functionality can be flexibly reprogrammed. From a technological perspective, our agile router's ability to avoid devastating reflected power echoes in networks should remove the need for currently used additional components (isolators, circulators, and in-line attenuators). From a more fundamental perspective, our simulations reveal a large broadening of the distribution of reflectionless scattering frequencies in the complex plane as the system becomes strongly overdamped. Without this effect, it is unlikely that functionalization of RSMs would be possible. We attribute this effect to differential absorption rates for different eigenstates based on their spatial distribution and also to increased eigenvalue interactions. A more quantitative theory for this broadening, based on rigorous scattering calculations, and statistical analysis to better understand these phenomena are an important avenue for future theoretical work in mesoscopic wave physics (see also note S4).

METHODS

Experimental setup

Our experimental setup is shown in Fig. 1B and is based on an electrically large irregularly shaped metallic box with dimensions 0.385 m by 0.422 m by 0.405 m. Sixteen percent of its boundaries are massively parametrized by two programmable metasurfaces, each comprising 152 meta-atoms. Each meta-atom has a 1-bit programmable reflection response that roughly mimics Dirichlet or Neumann boundary conditions for one field polarization (see fig. S1) (*75*). Each unit cell fuses two such meta-atoms, one rotated by 90°, and is hence 2-bit programmable (1 bit for each polarization), explaining the 2-bit color code used in Figs. 4 and 5A to visualize the metasurface configurations. Four single-mode guided scattering channels are connected to the system via waveguide-to-coax adapters, which are broadband impedance matched in free space (roughly frequency-flat reflection coefficient around −15 dB in free space; see fig. S2). The scattering system has a composite quality factor of 369, and 23 modes overlap at a given frequency. The average power transmitted between two scattering channels through our scattering system is −28.4 dB. Further details and characterizations of our setup are provided in note S1.

Our measurement apparatus can be switched between two measurement modalities: measuring the system's full scattering matrix with a VNA or performing in situ observations. The latter consists in injecting CW signals at f_1 and f_2, coherently controlled for f_1 in the case of Fig. 5, and measuring the power exiting our system through all connected channels with a spectrum analyzer. In situ observations are important to provide direct experimental evidence of the claimed routing functionalities, as opposed to relying on the linearity of the wave equation to use simulations based on measured scattering matrices. Further details can be found in note S1, including in fig. S5 a photographic image of the measurement apparatus underlying Fig. 5.

Calibration

To avoid that cables and other components of our measurement apparatus affect the characterization of our scattering system, we

perform multiple calibrations. First, the VNA is calibrated using a standard electronic calibration kit to remove the effect of propagation from the VNA ports to the circulators. Second, calibration measurements with the in situ measurement setup are performed to measure the signal attenuation due to the measurement apparatus. Specifically, we sequentially connect with an in-line SMA adapter each cable through which energy is injected directly to each possible cable through which energy exits. The received power on the spectrum analyzer, in this case, which does not involve propagation through the scattering system, serves as calibration of the measurement apparatus for in situ observations, and the corresponding measurements are plotted in light green in Figs. 3 (F to H), 4, and 5A. Further details are provided in note S2.

For the injection of the adapted wavefront in Fig. 5, we additionally perform a third calibration to determine relative amplitude and phase shifts between the two sources due to possible inaccuracies inside the multichannel coherent signal generator and/or differences in the cables between signal generator and scattering system. The detailed procedure is summarized in note S2.

Optimization

The identification of a metasurface configuration that yields a desired scattering response of our massively parametrized system is very challenging because no forward model exists to map a given metasurface configuration to the corresponding scattering response. Given the impossibility of accurate analytical forward models, training an artificial neural network to approximate a forward model may be possible in the future. This was already successfully achieved for weakly scattering perturbations in a multimode waveguide (*76*), similar to the setup from (*35*). However, the parametrization of scattering systems with strong reverberation such as ours is highly nonlinear because the impact of a given meta-atom on the scattering response depends on how the other meta-atoms are configured (*77*). Moreover, the 1-bit programmability severely limits gradient descent techniques because the tunable parameters can only be chosen from a discrete set rather than from a continuous range. Here, we therefore used a simple iterative trial-and-error algorithm based on VNA measurements of the system's scattering matrix to identify a suitable metasurface configuration. Details on the weights used to trade off the six constraints in the cost function and an algorithmic summary can be found in note S3. The identification of suitable metasurface configurations for various routing functionalities and operating frequency pairs can be performed offline in a calibration phase such that this optimization does not thwart the runtime deployment of our reflectionless programmable signal router.

Numerical study

The simulated structure in the inset of Fig. 2B is a two-dimensional, three-port rectangular cavity with three scatterers. The cavity dimensions are $L \times \frac{3}{4}L$ in the x-y plane. Similar to (*28*, *43*), we apply an impedance boundary condition at the walls of the cavity, which simulates a metallic wall followed by an infinite domain. The domain has a unit relative permeability and permittivity. We can alter the amount of absorption by the walls of the cavity by changing the conductivity: Lower values of conductivity correspond to increasingly absorptive walls. The scatterers are circular and perfectly conducting. For different ratios of absorption coupling to radiation coupling, we use an eigenfrequency solver to find the complex-valued reflection zeros of the scattering system using a PML method within a frequency interval from 50 to 75 c/L. Additional details, explanations, and results can be found in note S5.

Supplementary Materials

This PDF file includes:

Notes S1 to S5
Figs. S1 to S12

REFERENCES AND NOTES

1. M. Cai, O. Painter, K. J. Vahala, Observation of critical coupling in a fiber taper to a silica-microsphere whispering-gallery mode system. *Phys. Rev. Lett.* **85**, 74–77 (2000).
2. A. Yariv, Critical coupling and its control in optical waveguide-ring resonator systems. *IEEE Photon. Technol. Lett.* **14**, 483–485 (2002).
3. J. R. Tischler, M. S. Bradley, V. Bulović, Critically coupled resonators in vertical geometry using a planar mirror and a 5 nm thick absorbing film. *Opt. Lett.* **31**, 2045–2047 (2006).
4. N. I. Landy, S. Sajuyigbe, J. J. Mock, D. R. Smith, W. J. Padilla, Perfect metamaterial absorber. *Phys. Rev. Lett.* **100**, 207402 (2008).
5. V. S. Asadchy, I. A. Faniayeu, Y. Ra'di, S. A. Khakhomov, I. V. Semchenko, S. A. Tretyakov, Broadband reflectionless metasheets: Frequency-selective transmission and perfect absorption. *Phys. Rev. X* **5**, 031005 (2015).
6. D. M. Pozar, *Microwave Engineering* (John Wiley & Sons, 2009).
7. Y. D. Chong, L. Ge, H. Cao, A. D. Stone, Coherent perfect absorbers: Time-reversed lasers. *Phys. Rev. Lett.* **105**, 053901 (2010).
8. V. Grigoriev, A. Tahri, S. Varault, B. Rolly, B. Stout, J. Wenger, N. Bonod, Optimization of resonant effects in nanostructures via Weierstrass factorization. *Phys. Rev. A* **88**, 011803 (2013).
9. A. Krasnok, D. Baranov, H. Li, M.-A. Miri, F. Monticone, A. Alú, Anomalies in light scattering. *Adv. Opt. Photon.* **11**, 892–951 (2019).
10. W. Wan, Y. Chong, L. Ge, H. Noh, A. D. Stone, H. Cao, Time-reversed lasing and interferometric control of absorption. *Science* **331**, 889–892 (2011).
11. J. Zhang, K. F. MacDonald, N. I. Zheludev, Controlling light-with-light without nonlinearity. *Light Sci. Appl.* **1**, e18 (2012).
12. R. Bruck, O. L. Muskens, Plasmonic nanoantennas as integrated coherent perfect absorbers on SOI waveguides for modulators and all-optical switches. *Opt. Express* **21**, 27652–27671 (2013).
13. S. M. Rao, J. J. Heitz, T. Roger, N. Westerberg, D. Faccio, Coherent control of light interaction with graphene. *Opt. Lett.* **39**, 5345–5347 (2014).
14. Z. J. Wong, Y.-L. Xu, J. Kim, K. O'Brien, Y. Wang, L. Feng, X. Zhang, Lasing and anti-lasing in a single cavity. *Nat. Photon.* **10**, 796–801 (2016).
15. D. G. Baranov, A. Krasnok, T. Shegai, A. Alù, Y. Chong, Coherent perfect absorbers: Linear control of light with light. *Nat. Rev. Mater.* **2**, 17064 (2017).
16. Y. V. Fyodorov, S. Suwunnarat, T. Kottos, Distribution of zeros of the *S*-matrix of chaotic cavities with localized losses and coherent perfect absorption: Non-perturbative results. *J. Phys. Math. Theor.* **50**, 30LT01 (2017).
17. H. Li, S. Suwunnarat, R. Fleischmann, H. Schanz, T. Kottos, Random matrix theory approach to chaotic coherent perfect absorbers. *Phys. Rev. Lett.* **118**, 044101 (2017).
18. H. Li, S. Suwunnarat, T. Kottos, Statistical design of chaotic waveforms with enhanced targeting capabilities. *Phys. Rev. B* **98**, 041107 (2018).
19. Y. V. Fyodorov, M. Osman, Eigenfunction non-orthogonality factors and the shape of CPA-like dips in a single-channel reflection from lossy chaotic cavities. *J. Phys. Math. Theor.* **55**, 224013 (2022).
20. K. Pichler, M. Kühmayer, J. Böhm, A. Brandstötter, P. Ambichl, U. Kuhl, S. Rotter, Random anti-lasing through coherent perfect absorption in a disordered medium. *Nature* **567**, 351–355 (2019).
21. L. Chen, T. Kottos, S. M. Anlage, Perfect absorption in complex scattering systems with or without hidden symmetries. *Nat. Commun.* **11**, 5826 (2020).
22. M. F. Imani, D. R. Smith, P. del Hougne, Perfect absorption in a disordered medium with programmable meta-atom inclusions. *Adv. Funct. Mater.* **30**, 2005310 (2020).
23. J. Sol, D. R. Smith, P. del Hougne, Meta-programmable analog differentiator. *Nat. Commun.* **13**, 1713 (2022).
24. B. W. Frazier, T. M. Antonsen, S. M. Anlage, E. Ott, Wavefront shaping with a tunable metasurface: Creating cold spots and coherent perfect absorption at arbitrary frequencies. *Phys. Rev. Res.* **2**, 043422 (2020).
25. P. del Hougne, K. B. Yeo, P. Besnier, M. Davy, On-demand coherent perfect absorption in complex scattering systems: Time delay divergence and enhanced sensitivity to perturbations. *Laser Photon. Rev.* **15**, 2000471 (2021).

26. P. del Hougne, K. B. Yeo, P. Besnier, M. Davy, Coherent wave control in complex media with arbitrary wavefronts. *Phys. Rev. Lett.* **126**, 193903 (2021).
27. T. J. Cui, M. Q. Qi, X. Wan, J. Zhao, Q. Cheng, Coding metamaterials, digital metamaterials and programmable metamaterials. *Light Sci. Appl.* **3**, –e218 (2014).
28. M. Dupré, P. del Hougne, M. Fink, F. Lemoult, G. Lerosey, Wave-field shaping in cavities: Waves trapped in a box with controllable boundaries. *Phys. Rev. Lett.* **115**, 017701 (2015).
29. W. R. Sweeney, C. W. Hsu, A. D. Stone, Theory of reflectionless scattering modes. *Phys. Rev. A* **102**, 063511 (2020).
30. A.-S. B.-B. Dhia, L. Chesnel, V. Pagneux, Trapped modes and reflectionless modes as eigenfunctions of the same spectral problem. *Proc. R. Soc. A.* **474**, 20180050 (2018).
31. A. D. Stone, W. R. Sweeney, C. W. Hsu, K. Wisal, Z. Wang, Reflectionless excitation of arbitrary photonic structures: A general theory. *Nanophoton.* **10**, 343–360 (2020).
32. A. A. Gorbatsevich, N. M. Shubin, Unified theory of resonances and bound states in the continuum in Hermitian tight-binding models. *Phys. Rev. B* **96**, 205441 (2017).
33. Y. Elesin, B. S. Lazarov, J. S. Jensen, O. Sigmund, Time domain topology optimization of 3D nanophotonic devices. *Photon. Nanostruct. - Fundam. Appl* **12**, 23–33 (2014).
34. A. Y. Piggott, J. Lu, K. G. Lagoudakis, J. Petykiewicz, T. M. Babinec, J. Vučković, Inverse design and demonstration of a compact and broadband on-chip wavelength demultiplexer. *Nat. Photon.* **9**, 374–377 (2015).
35. R. Bruck, K. Vynck, P. Lalanne, B. Mills, D. J. Thomson, G. Z. Mashanovich, G. T. Reed, O. L. Muskens, All-optical spatial light modulator for reconfigurable silicon photonic circuits. *Optica* **3**, 396–402 (2016).
36. J. Leuthold, C. H. Joyner, Multimode interference couplers with tunable power splitting ratios. *J. Light. Technol.* **19**, 700–707 (2001).
37. S. Nagai, G. Morishima, H. Inayoshi, K. Utaka, Multimode interference photonic switches (MIPS). *J. Light. Technol.* **20**, 675–681 (2002).
38. A. M. Al-hetar, A. B. Mohammad, A. S. M. Supa'at, Z. A. Shamsan, I. Yulianti, Fabrication and characterization of polymer thermo-optic switch based on mmi coupler. *Opt. Commun.* **284**, 1181–1185 (2011).
39. D. A. May-Arrioja, P. LiKamWa, J. J. Sánchez-Mondragón, R. J. Selvas-Aguilar, I. Torres-Gomez, A reconfigurable multimode interference splitter for sensing applications. *Meas. Sci. Technol.* **18**, 3241–3246 (2007).
40. X. Zhang, C. Meng, Z. Yang, Wave manipulations by coherent perfect channeling. *Sci. Rep.* **7**, 13907 (2017).
41. O. Richoux, V. Achilleos, G. Theocharis, I. Brouzos, Subwavelength interferometric control of absorption in three-port acoustic network. *Sci. Rep.* **8**, 12328 (2018).
42. O. Richoux, V. Achilleos, G. Theocharis, I. Brouzos, F. Diakonos, Multi-functional resonant acoustic wave router. *J. Phys. Appl. Phys.* **53**, 235101 (2020).
43. M. F. Imani, S. Abadal, P. del Hougne, Metasurface-programmable wireless network-on-chip. *Adv. Sci.* **9**, 2201458 (2022).
44. I. Rotter, E. Persson, K. Pichugin, P. Šeba, Spectroscopic studies in open quantum systems. *Phys. Rev. E* **62**, 450–461 (2000).
45. E. Persson, I. Rotter, H.-J. Stöckmann, M. Barth, Observation of resonance trapping in an open microwave cavity. *Phys. Rev. Lett.* **85**, 2478–2481 (2000).
46. M. Asano, K. Y. Bliokh, Y. P. Bliokh, A. G. Kofman, R. Ikuta, T. Yamamoto, Y. S. Kivshar, L. Yang, N. Imoto, Ş. K. Özdemir, F. Nori, Anomalous time delays and quantum weak measurements in optical micro-resonators. *Nat. Commun.* **7**, 13488 (2016).
47. Y. Kang, A. Z. Genack, Transmission zeros with topological symmetry in complex systems. *Phys. Rev. B* **103**, L100201 (2021).
48. L. Chen, S. M. Anlage, Y. V. Fyodorov, Generalization of Wigner time delay to subunitary scattering systems. *Phys. Rev. E* **103**, L050203 (2021).
49. L. Chen, S. M. Anlage, Use of transmission and reflection complex time delays to reveal scattering matrix poles and zeros: Example of the ring graph. *Phys. Rev. E* **105**, 054210 (2022).
50. L. Chen, S. M. Anlage, Y. V. Fyodorov, Statistics of complex Wigner time delays as a counter of *S*-matrix poles: Theory and experiment. *Phys. Rev. Lett.* **127**, 204101 (2021).
51. Y. Huang, Y. Kang, A. Z. Genack, Wave excitation and dynamics in non-Hermitian disordered systems. *Phys. Rev. Res.* **4**, 013102 (2022).
52. P. W. Brouwer, K. M. Frahm, C. W. J. Beenakker, Quantum mechanical time-delay matrix in chaotic scattering. *Phys. Rev. Lett.* **78**, 4737–4740 (1997).
53. M. del Hougne, S. Gigan, P. del Hougne, Deeply subwavelength localization with reverberation-coded aperture. *Phys. Rev. Lett.* **127**, 043903 (2021).
54. A. Ø. Svela, J. M. Silver, L. Del Bino, S. Zhang, M. T. M. Woodley, M. R. Vanner, P. Del'Haye, Coherent suppression of backscattering in optical microresonators. *Light Sci. Appl.* **9**, 204 (2020).
55. Y. D. Chong, A. D. Stone, Hidden black: Coherent enhancement of absorption in strongly scattering media. *Phys. Rev. Lett.* **107**, 163901 (2011).
56. G. K. Shirmanesh, R. Sokhoyan, P. C. Wu, H. A. Atwater, Electro-optically tunable multifunctional metasurfaces. *ACS Nano* **14**, 6912–6920 (2020).
57. Y. Eliezer, U. Ruhrmair, N. Wisiol, S. Bittner, H. Cao, Exploiting structural nonlinearity of a reconfigurable multiple-scattering system. arXiv:2208.08906 (2022).
58. J.-M. Hannula, J. Holopainen, V. Viikari, Concept for frequency-reconfigurable antenna based on distributed transceivers. *IEEE Antennas Wirel. Propag. Lett.* **16**, 764–767 (2017).
59. T. Sleasman, M. F. Imani, A. V. Diebold, M. Boyarsky, K. P. Trofatter, D. R. Smith, Implementation and characterization of a two-dimensional printed circuit dynamic metasurface aperture for computational microwave imaging. *IEEE Trans. Antennas Propag.* **69**, 2151–2164 (2020).
60. S. Mignuzzi, S. Vezzoli, S. A. R. Horsley, W. L. Barnes, S. A. Maier, R. Sapienza, Nanoscale design of the local density of optical states. *Nano Lett.* **19**, 1613–1617 (2019).
61. T. Kottos, U. Smilansky, Chaotic scattering on graphs. *Phys. Rev. Lett.* **85**, 968–971 (2000).
62. Y. Shen, N. C. Harris, S. Skirlo, M. Prabhu, T. Baehr-Jones, M. Hochberg, X. Sun, S. Zhao, H. Larochelle, D. Englund, M. Soljačić, Deep learning with coherent nanophotonic circuits. *Nat. Photon.* **11**, 441–446 (2017).
63. O. N. Dorokhov, On the coexistence of localized and extended electronic states in the metallic phase. *Solid State Commun.* **51**, 381–384 (1984).
64. C. W. J. Beenakker, Random-matrix theory of quantum transport. *Rev. Mod. Phys.* **69**, 731–808 (1997).
65. B. Gérardin, J. Laurent, A. Derode, C. Prada, A. Aubry, Full transmission and reflection of waves propagating through a maze of disorder. *Phys. Rev. Lett.* **113**, 173901 (2014).
66. R. Sarma, A. G. Yamilov, S. Petrenko, Y. Bromberg, H. Cao, Control of energy density inside a disordered medium by coupling to open or closed channels. *Phys. Rev. Lett.* **117**, 086803 (2016).
67. C. Wang, W. R. Sweeney, A. D. Stone, L. Yang, Observation of coherent perfect absorption at an exceptional point. *Science* **373**, 1261–1265 (2021).
68. C. Ferise, P. del Hougne, S. Félix, V. Pagneux, M. Davy, Exceptional points of *PT*-symmetric reflectionless states in complex scattering systems. *Phys. Rev. Lett.* **128**, 203904 (2022).
69. Z. Hayran, F. Monticone, Challenging fundamental limitations in electromagnetics with time-varying systems. arXiv:2205.07142 (2022).
70. D. G. Baranov, A. Krasnok, A. Alù, Coherent virtual absorption based on complex zero excitation for ideal light capturing. *Optica* **4**, 1457 (2017).
71. G. Trainiti, Y. Ra'di, M. Ruzzene, A. Alù, Coherent virtual absorption of elastodynamic waves. *Sci. Adv.* **5**, eaaw3255 (2019).
72. A. Farhi, A. Mekawy, A. Alù, D. Stone, Excitation of absorbing exceptional points in the time domain. *Phys. Rev. A* **106**, L031503 (2022).
73. L.-P. Euve, P. Petitjeans, A. Maurel, V. Pagneux, Transient total absorption for water waves: A two port setup. *Bull. Am. Phys. Soc.* **66**, (2021).
74. Z. Zhou, Y. Li, E. Nahvi, H. Li, Y. He, I. Liberal, N. Engheta, General impedance matching via doped epsilon-near-zero media. *Phys. Rev. Appl.* **13**, 034005 (2020).
75. N. Kaina, M. Dupré, M. Fink, G. Lerosey, Hybridized resonances to design tunable binary phase metasurface unit cells. *Opt. Express* **22**, 18881–18888 (2014).
76. N. J. Dinsdale, P. R. Wiecha, M. Delaney, J. Reynolds, M. Ebert, I. Zeimpekis, D. J. Thomson, G. T. Reed, P. Lalanne, K. Vynck, O. L. Muskens, Deep learning enabled design of complex transmission matrices for universal optical components. *ACS Photon.* **8**, 283–295 (2021).
77. C. Saigre-Tardif, P. del Hougne, Self-adaptive RISs beyond free space: convergence of localization, sensing and communication under rich-scattering conditions. arXiv:2205.11186 (2022).

Acknowledgments: A.D.S. acknowledges useful discussions with M. Fink and F. Lemoult. P.d.H. acknowledges stimulating discussions with S. A. R. Horsley, D. B. Phillips, and R. Sapienza. The metasurface prototypes were purchased from Greenerwave. **Funding:** J.S. and P.d.H. acknowledge funding from the CNRS prématuration program (project "MetaFilt"), the European Union's European Regional Development Fund, and the French region of Brittany and Rennes Métropole through the contrats de plan État-Région program (project "SOPHIE STIC & Ondes"). A.A. and A.D.S. acknowledge funding from the Simons Collaboration on Extreme Wave Phenomena and the NSF Condensed Matter and Materials Theory (CMMT) program under grant no. DMR-1743235. **Author contributions:** A.D.S. and P.d.H. conceived the project. J.S. and P.d.H. conducted the experiments. A.A. and A.D.S. conducted the numerical simulations. All authors interpreted the results and contributed with thorough discussions. P.d.H. wrote the manuscript. **Competing interests:** The authors declare that they have no competing interests. **Data and materials availability:** All data needed to evaluate the conclusions in the paper are present in the paper and/or the Supplementary Materials.

Submitted 24 September 2022
Accepted 21 December 2022
Published 25 January 2023
10.1126/sciadv.adf0323

ScienceAdvances

Reflectionless programmable signal routers

Jrme Sol, Ali Alhulaymi, A. Douglas Stone, and Philipp del Hougne

Sci. Adv., **9** (4), eadf0323.
DOI: 10.1126/sciadv.adf0323

Science Advances (ISSN) is published by the American Association for the Advancement of Science. 1200 New York Avenue NW, Washington, DC 20005. The title *Science Advances* is a registered trademark of AAAS.